SOME SINGULARITIES OF SUPERSONIC UNDEREXPANDED JET INTERACTION WITH A PLANE OBSTACLE

I. P. Ginzburg, B. G. Semiletenko,
V. S. Terpigor'ev, and V. N. Uskov

UDC 533.601.1

Results are presented of an experimental investigation of the interaction between a supersonic underexpanded jet and an obstacle mounted at various distances from the nozzle exit. It is shown that for certain distances h unstable modes of flow around the obstacle are observed for Ma = 2.18, n = 1.9, $3.6 < h < 5.6$, say.

A number of papers [1-3] investigating the interaction between an underexpanded supersonic jet impinging on an infinite flat obstacle mounted at a short range from the nozzle exit perpendicularly to the jet axis when the static-pressure maximum is at the center of the obstacle has recently appeared. In this case the typical diagram of the shock location is that presented in Fig. 1. A central compression shock 2 develops ahead of the obstacle, and by intersecting the hanging shock of the free jet 1 results in the formation of the reflected shock 3. The subsonic flow behind the central shock is separated from the customarily supersonic flow behind the reflected shock by the surface of tangential discontinuity 4. The reflected shock 3 emerges at the point B on the jet boundary, causing a discontinuity and intense jet spreading in the form of a fan jet along the obstacle surface.

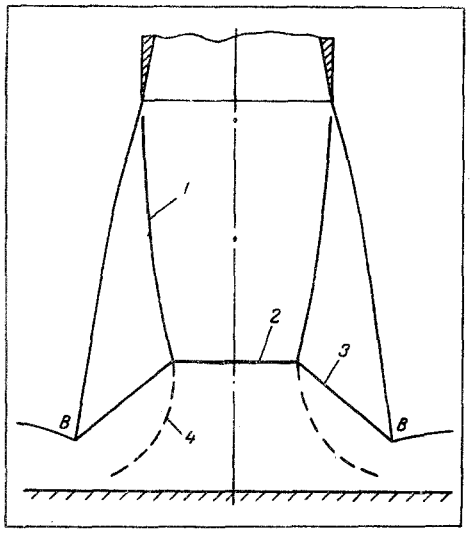

Fig. 1. Diagram of the wave configuration for supersonic underexpanded jet interaction with an obstacle: 1, 2, 3) hanging, central, and reflected compression shocks, respectively; 4) tangential discontinuity.

As the obstacle recedes from the nozzle exit, an "acoustic vibration" mode can set in, whose origination and mechanism have still not been fully studied. The physical picture of the flow has also not been clarified in the case when the maximum value of the static pressure holds on the periphery rather than at the center of the obstacle.

Experimental investigations of the interaction between a jet and an unbounded flat obstacle were conducted to clarify these complex questions. Supersonic air jets were investigated for different Mach numbers at the nozzle exit Ma = 1.5-2.5, degrees of off-design n = 1.5-12, and ranges $\bar{h} \geq 3$ from the nozzle exit. By using the optical instrument IAB-451, the wave configuration of the jet interaction with the obstacle was photographed. The obstacle had an orifice of 0.3 mm diameter for measurement of the static pressure. The total pressure was measured by using a miniature Pitot tube, whose opening had a rectangular shape of 1.6×0.08 mm^2 size and a 0.06 mm wall thickness. The pressure was measured by DD-10 inductive transducers in combination with an ID-21 measuring unit and the results recorded on an N-109 loop oscillograph. To obtain a continuous static and total pressure distribution, the obstacle was displaced in its plane at a 6 mm/sec velocity during the blowing. The obstacle displacement was recorded by a path

Leningrad Mechanical Institute. Translated from Inzhenerno-Fizicheskii Zhurnal, Vol. 19, No. 3, pp. 412-417, September, 1970. Original article submitted April 22, 1970.

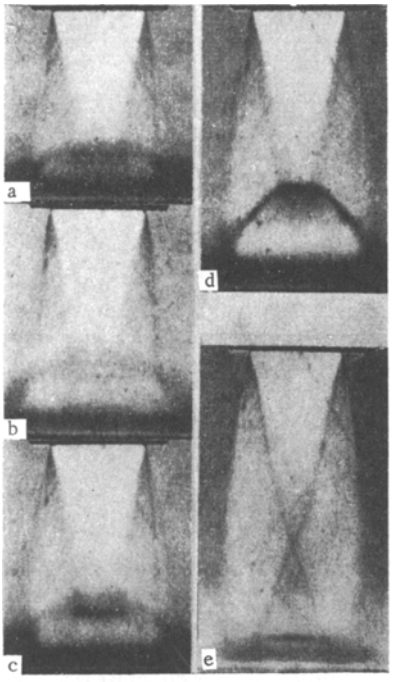

Fig. 2

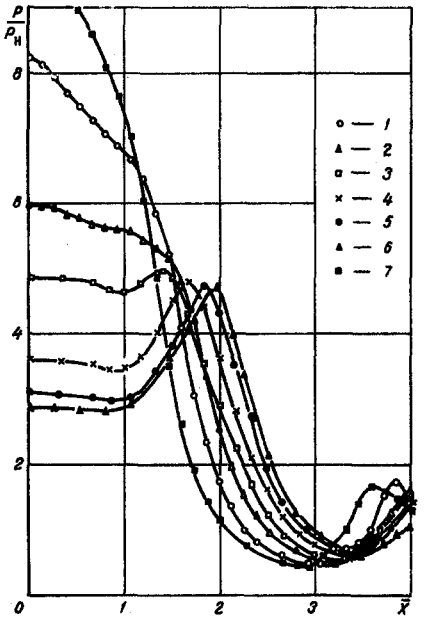

Fig. 3

Fig. 2. Toepler photographs of jet interaction with an obstacle: a) $\bar{h} = 4$; b) 4.8; c) 5.0; d) 6.0; e) 6.8.

Fig. 3. Static-pressure distribution over the obstacle surface: 1) $\bar{h} = 2.8$; 2) 3.6; 3) 4.0; 4) 5.2; 5) 6.0; 6) 6.6; 7) 6.8.

transducer after 0.5 mm of obstacle motion. The total measurement error, including oscillogram processing, did not exceed 4%.

The flow in the boundary layer near the wall on the obstacle was visualized by using injection of anti-freeze (spindle oil). The stream direction on the obstacle was determined visually by the direction of oil-film spreading. Besides the injection of anti-freeze to visualize the flow, wire probes were also mounted in the stream, which also permitted estimation of the flow direction. By using the wire probes a qualitative picture of the gas flow was successfully obtained, even outside the boundary layer near the wall.

Insofar as the qualitative picture of jet interaction with an obstacle was observed in the investigated range of variation of the jet parameters and the range $\bar{h}$, then the data obtained for Ma = 2.185, $\vartheta_a = 5°$, $r_a = 15$ mm, n = 1.9 are henceforth presented to illustrate the results. The range $\bar{h}$ between the nozzle exit section and the obstacle varied from 2.8 to 6.8 in 0.4 steps. Typical results of the experiments are presented in Figs. 2-5.

It is seen from the graphs in Fig. 3 that the static-pressure curve has a maximum at the center of the obstacle up to the range $\bar{h} \leq 3.6$, and drops gradually to the periphery down to the possible zone of jet boundary-layer separation from the obstacle surface.

A peripheral static-pressure maximum appears on the obstacle at the range $\bar{h} > 3.6$. Hence, the pressure at the center of the obstacle drops as $\bar{h}$ increases, and the peripheral pressure maximum changes slightly in magnitude. This can be explained by the fact that ahead of the central compression shock the Mach number increases as $\bar{h}$ increases, and therefore, the total pressure losses grow and the pressure at the center of the obstacle decreases. The total pressure losses of the gas which has passed the oblique compression shocks 1 and 3 (Fig. 1) remain less than for the gas which has passed the central shock. Moreover, since the gas discharge through the shock 3 increases and through the central shock 2 diminishes as the range $\bar{h}$ grows, then the line of tangential discontinuity 4 approaches closer and closer to the obstacle surface.

Because of the reasons mentioned, the mixing zone of the streams being developed along the tangential discontinuity is closed at some $\bar{h}$ on the obstacle surface and results in the appearance of a peripheral

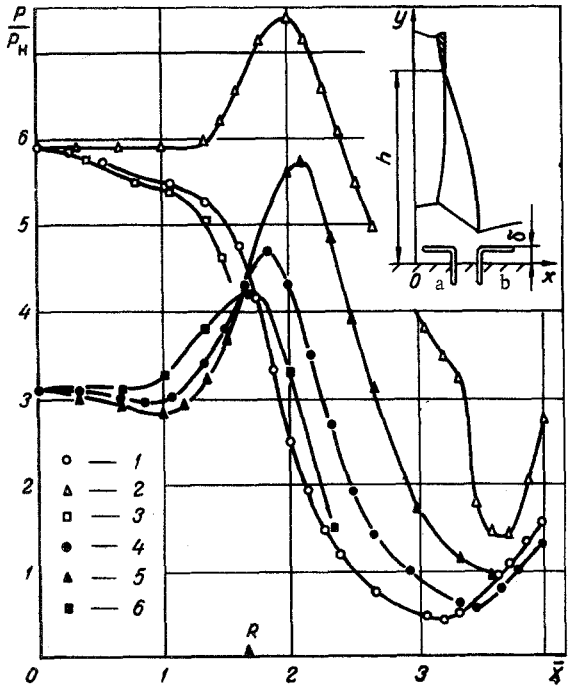

Fig. 4

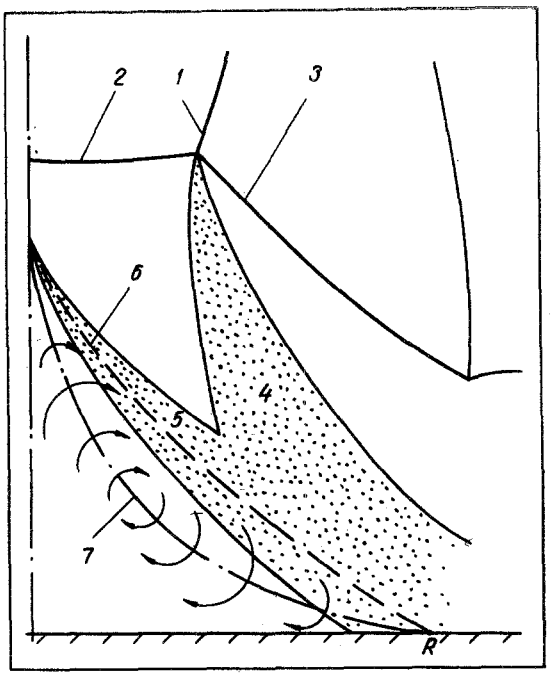

Fig. 5

Fig. 4. Static-pressure and stagnation-pressure distributions along the obstacle: 1, 2, 3) $\bar{h} = 3.6$, $\delta = 0.5$ mm; 4, 5, 6) $\bar{h} = 6.0$, $\delta = 0.1$ mm. 1, 4) Static pressure; 2, 5) stagnation pressure for the Pitot tube at a; 3, 6) stagnation pressure for the Pitot tube at b; R) spreading point determined in a visualization for $\bar{h} = 6.0$.

Fig. 5. Diagram of the flow in the stationary mode and in the presence of a maximum peripheral pressure: 1, 2, 3) hanging, central, and reflected compression shocks; 4, 5) mixing zones; 6) separating streamline; 7) line of zero longitudinal velocities.

static-pressure maximum at the obstacle. Part of the gas which has passed the central compression shock is hence drawn into the mixing zone and leaves the central domain, while another part cannot overcome the peripheral maximum pressure and accumulates in the central domain. The pressure therein rises and the central shock 2 starts to be displaced upstream until the pressure behind it becomes somewhat greater than the peripheral maximum. Then the gas accumulated in the central domain of the obstacle has the opportunity to leave it; the pressure behind the central shock drops and it starts to move downstream to its initial position. The process is later duplicated and nonstationary jet interaction with the obstacle is realized. The shock displacements occur at high frequency, hence, the jet wave configuration on the Toepler photographs becomes diffuse (Fig. 2b, c).

As $\bar{h}$ increases further, the shock standoff from the obstacle and the length of the mixing zone increase, a greater and greater portion of the gas which has passed the shock (Fig. 1) is entrained into the mixing zone by the gas stream and leaves the central domain of the obstacle. The amplitude and frequency of fluctuation of the shock 2 diminish (Fig. 2c). At some $\bar{h}$ all the gas which has passed the central compression shock leaves the central domain because of mixing with the peripheral stream. The jet interaction with the obstacle becomes stable (Fig. 2d).

Flow visualization by using fluid injection and wire probes showed that there is a reverse flow to the center of the obstacle in this case. Results of measuring the stagnation pressure (Fig. 4) also indicate this. If the pressure measured with the Pitot tube suggests the presence of flow from the center in regimes prior to the appearance of instability ($\bar{h} < 4$), then the results of stagnation-pressure measurements corresponding to stationary flow around an obstacle in the presence of a peripheral maximum for $\bar{h} \geq 5.6$ indicate flow toward the center of the obstacle (Fig. 4). The position of the spreading line, bounding the reverse-flow domain to the center of the obstacle and defined by the equality of the static and total pressures, practically coincides with the results visualized by injection of anti-freeze (Fig. 4, point R).

A simplified flow configuration corresponding to stationary interaction between a jet and obstacle is pictured in Fig. 5 in the presence of a peripheral maximum pressure. The gas which has passed the central compression shock 2, having been developed in the mixing zone 4 along the surface of tangential discontinuity is mixed with the gas which has passed the shock 3. Its total pressure hence increases so much that it can overcome the peripheral static-pressure maximum and leave the central domain of the obstacle. However, a part of the gas from the mixing domain 5 unrolls around the line of spreading R and flows to the center of the obstacle to form a stagnant vortical flow. The gas from the stagnant domain is mixed in zone 5 with the stream which has passed the central compression shocks, and then with the peripheral stream in zone 4 also. Hence, part of the gas from the stagnant domain leaves, and a new batch of gas enters the stagnant zone from the line of spreading R.

A similar flow configuration holds up to the range $\bar{h} < 6.8$, after which jump changes occur in both the jet wave configuration ahead of the obstacle (Fig. 2e) and in the static-pressure diagram (Fig. 3, curve 7). A compression shock originates in the jet ahead of the obstacle at a short distance from the obstacle surface, and the jet wave configuration within the first barrel corresponds to the wave configuration of a free submerged jet. The static-pressure distribution is characterized by a maximum at the center of the obstacle (Fig. 3, curve 7) and there is no return flow to the central domain of the obstacle.

The detailed experimental investigation conducted permits giving a sufficiently clear description of the qualitative picture of supersonic jet interaction with a flat obstacle for various distances between the obstacle and the nozzle exit, which will later allow construction of a mathematical scheme to analyze the interaction mentioned and the origination of unstable modes.

NOTATION

x	is the distance along the obstacle from the central point;
h	is the distance from the nozzle exit to the obstacle;
r_a	is the radius of the nozzle exit section;
$\bar{X} = x/r_a$, $\bar{h} = h/r_a$	
Ma	is the Mach number at the nozzle exit;
ϑ_a	is the nozzle aperture angle;
$n = P_a/P_H$	is the degree of off-design;
P_a	is the pressure at the nozzle exit;
P_H	is the pressure in the ambient medium.

LITERATURE CITED

1. I. P. Ginzburg, I. A. Belov, G. A. Akimov, and V. S. Terpigor'ev, Transactions of the Scientific-Technical Society [in Russian], Leningrad Mechanical Institute, Leningrad (1967).
2. I. P. Ginzburg, I. A. Belov, V. S. Terpigor'ev, and L. I. Shub, Transactions of the Scientific-Technical Society [in Russian], Leningrad Mechanical Institute, Leningrad (1968).
3. V. A. Pogorelov, Inzh.-Fiz. Zh., 17, No. 6 (1969).